Eur. Phys. J. A (2022) 58:15
https://doi.org/10.1140/epja/s10050-022-00673-2

THE EUROPEAN PHYSICAL JOURNAL A

Regular Article - Theoretical Physical

Collision system size dependence of light (anti-)nuclei and (anti-)hypertriton production in high energy nuclear collisions

Zhi-Lei She[1,2], **Liang Zheng**[2], **Dai-Mei Zhou**[3], **Yi-Long Xie**[2], **Hong-Ge Xu**[2], **Gang Chen**[2,a]

[1] Institute of Geophysics and Geomatics, China University of Geosciences, Wuhan 430074, China
[2] School of Mathematics and Physics, China University of Geosciences, Wuhan 430074, China
[3] Institute of Particle Physics, Central China Normal University, Wuhan 430079, China

Received: 30 October 2021 / Accepted: 23 January 2022 / Published online: 3 February 2022

Communicated by Che-Ming Ko

Abstract The collision system size dependence of light (anti-)nuclei and (anti-)hypertriton production is investigated using the parton and hadron cascade (PACIAE) model plus dynamically constrained phase-space coalescence (DCPC) model in ^{10}B+^{10}B, ^{12}C+^{12}C, ^{16}O+^{16}O, ^{20}Ne+^{20}Ne, ^{27}Al+^{27}Al, ^{40}Ar+^{40}Ar, ^{63}Cu+^{63}Cu, ^{96}Ru+^{96}Ru, ^{197}Au+^{197}Au, and ^{238}U+^{238}U collisions at $\sqrt{s_{\rm NN}}$ = 200 GeV. The yield ratios of deuteron to proton, helium-3 to proton, hypertriton to Λ-hyperon are predicted for various collision systems. In this study, we find the yield ratios between anti-(hyper-)nuclei are significantly suppressed compared to the ratios between the (hyper-)nuclei. It is also interesting to see the strangeness population factor s_3 shows a non-smooth dependence of atomic mass number A around 12 to 27, which can be related to the relative size of the produced nuclei and the emission source of different collision systems. Our present study provides a reference for a upcoming collision system scan program at RHIC.

1 Introduction

Over the last few years, high energy nuclear collisions experiments have led to a rapid development on the study of light nuclei and hypernuclei production [1–3], such as the search for the Quantum Chromdynamics (QCD) critical point by light nuclei [4,5], the precise measurement of the fundamental charge-parity-time reversal (CPT) theorem using hypertriton ($^3_\Lambda$H) with its corresponding anti-hypertriton ($^{\overline{3}}_{\overline{\Lambda}}\overline{\rm H}$) [6,7] and the clues for the discovery of light anti-nuclei in cosmic rays [8,9]. Light (hyper-)nuclei with baryon number $B \leq 4$, i.e., deuteron (d), helium-3 (^{3}He), triton (^{3}H), hypertriton ($^3_\Lambda$H), helium-4 (^{4}He) and their antiparticles, have been discovered and studied at the Relativistic Heavy Ion Collider (RHIC) and the Large Hadron Collider (LHC) [10–15].

Light nuclei production has been investigated with various theoretical methods like the statistical thermal method [16–19], the coalescence model [20–23] and the transport model [24–27]. Lots of efforts have been devoted to the study of light (anti-)nuclei and (anti-)hypernuclei production in terms of their yields, transverse momentum spectra, collective flow, etc. However, the underlying production mechanism of light (anti-)(hyper-)nuclei in nuclear reactions is still not fully understood [1–3].

Recently, several proposals for collision system scans have been made to study the possible signals of the quark gluon plasma (QGP) matter and other physical properties at RHIC [28–31] and LHC energies [32–34], where their bulk properties and multi-particle correlation observables are discussed at the final-state hadron level. In this work, a scan of symmetric nuclear collision systems is proposed, including ^{10}B+^{10}B, ^{12}C+^{12}C, ^{16}O+^{16}O, ^{20}Ne+^{20}Ne, ^{27}Al+^{27}Al, ^{40}Ar+^{40}Ar, ^{63}Cu+^{63}Cu, ^{96}Ru+^{96}Ru, ^{197}Au+^{197}Au, and ^{238}U+^{238}U at the top RHIC energies of $\sqrt{s_{\rm NN}}$ = 200 GeV.

In this paper, we investigate the light (anti-)nuclei and (anti-)hypertriton production in the nuclear system size scan program from ^{10}B+^{10}B to ^{238}U+^{238}U in the most central collisions at $\sqrt{s_{\rm NN}}$ = 200 GeV, by using the dynamically constrained phase-space coalescence (DCPC) model [35] with the needed final-state hadrons generated by the parton and hadron cascade (PACIAE) model [36]. Specifically, the integrated yields dN/dy of d ($\overline{\rm d}$), ^{3}He ($^{\overline{3}}\overline{\rm He}$), ^{3}H ($^{\overline{3}}\overline{\rm H}$), and $^3_\Lambda$H ($^{\overline{3}}_{\overline{\Lambda}}\overline{\rm H}$) are predicted. Then, we present the yield ratios of d/p ($\overline{\rm d}/\overline{\rm p}$), ^{3}He/p ($^{\overline{3}}\overline{\rm He}/\overline{\rm p}$), and ^{3}H/p ($^{\overline{3}}\overline{\rm H}/\overline{\rm p}$) for light (anti-)nuclei in different symmetric collision systems. Furthermore, the system size A dependence of $^3_\Lambda$H/Λ ($^{\overline{3}}_{\overline{\Lambda}}\overline{\rm H}/\overline{\Lambda}$) and the strangeness population factor s_3 ($\overline{s_3}$) for (anti-)hypertriton are also discussed.

[a] e-mail: chengang1@cug.edu.cn (corresponding author)

In the next section, Sect. 2, the PACIAE and DCPC model are briefly introduced. The predictions for light (anti-)nuclei and (anti-)hypertriton production in the scan of nuclear collision systems are given in the Sect. 3. The last section summarizes the conclusions.

2 Models

In this work, the high energy nuclear collisions are simulated to generate the phase-space distribution of final-state particles by the PACIAE model [36] with version 2.2b, which can be employed to simulate high energy nucleus-nucleus (AA), proton-nucleus (pA), and proton-proton (pp) collisions.

The PACIAE model is based on the parton initiation described by PYTHIA 6.4 convoluted with the nuclear geometry and the Glauber model [37]. And then the partonic rescattering is introduced by the $2 \to 2$ LO-pQCD parton-parton cross sections [38]. Then the hadronization conducts through the Lund string fragmentation [37] or the phenomenological coalescence model [36]. The hadron rescattering process happens until the hadronic freeze-out. Here, we assume that the hyperons heavier than Λ have already decayed before the creation of light (hyper-)nuclei.

The DCPC model [35] in this work is employed to calculate production of light (anti-)nuclei and (anti-)hypernuclei, which was successfully applied in different collision systems at RHIC and LHC, e.g., pp [39,40], Cu + Cu [41,42], Au + Au [43–46], and Pb + Pb [47,48] collisions. In this approach, we can estimate the yield of a single particle in the six-dimension phase space by an integral

$$Y_1 = \int_{H \leqslant E} \frac{\mathrm{d}\vec{q}\,\mathrm{d}\vec{p}}{h^3}, \tag{1}$$

where H and E represent the Hamiltonian and energy of the particle, respectively. Similarly, the yield of N particle cluster can also be calculated by the following integral

$$Y_N = \int \ldots \int_{H \leqslant E} \frac{\mathrm{d}\vec{q}_1\mathrm{d}\vec{p}_1 \ldots \mathrm{d}\vec{q}_N\mathrm{d}\vec{p}_N}{h^{3N}}. \tag{2}$$

Additionally, Eq. (2) must satisfied the following constraint conditions

$$m_0 \leqslant m_{inv} \leqslant m_0 + \Delta m, \tag{3}$$

$$|\vec{q}_{ij}| \leqslant D_0, (i \neq j; i, j = 1, 2, \ldots, N). \tag{4}$$

where

$$m_{inv} = \left[\left(\sum_{i=1}^{N} E_i \right)^2 - \left(\sum_{i=1}^{N} \vec{p}_i \right)^2 \right]^{1/2}, \tag{5}$$

E_i, $\vec{p}_i$(i=1,2,…,N) are respectively the energy and momentum of the particles to be combined to form the nuclei. m_0 and D_0 stand for the rest mass and diameter of light (anti-)nuclei or (anti-)hypernuclei. The radius values R = 1.92, 1.74, 1.61, 5.0 fm are selected for d ($\bar{\mathrm{d}}$), ^{3}He ($^3\overline{\mathrm{He}}$), ^{3}H ($^3\overline{\mathrm{H}}$), and $^3_\Lambda$H ($^3_{\overline{\Lambda}}\overline{\mathrm{H}}$) [2,49] in this simulation, respectively. Δm denotes the allowed mass uncertainty, and $|\vec{q}_{ij}|$ is the distance between particles i and j.

For the following results we fixed a suitable set of parameters of PACIAE+DCPC model, suggested in Ref. [35], with a fit to the experimental data at RHIC in Refs. [10,11,50–53]. This allows us to predict light (anti-)(hyper-)nuclei production for the scan of nuclear systems involving 0-10% centrality collisions from ^{10}B+^{10}B to ^{238}U+^{238}U at $\sqrt{s_{\mathrm{NN}}}$ = 200 GeV, and the selected particles, p ($\bar{\mathrm{p}}$), Λ ($\overline{\Lambda}$), d ($\bar{\mathrm{d}}$), ^{3}He ($^3\overline{\mathrm{He}}$), ^{3}H ($^3\overline{\mathrm{H}}$), and $^3_\Lambda$H ($^3_{\overline{\Lambda}}\overline{\mathrm{H}}$), with the kinetic windows, pseudo-rapidity $|\eta| < 0.5$, and transverse momentum $0 < p_T < 6.0$ GeV/c.

3 Results and discussion

Figure 1 shows the integrated yields dN/dy of p ($\bar{\mathrm{p}}$), Λ ($\overline{\Lambda}$), d ($\bar{\mathrm{d}}$), ^{3}He ($^3\overline{\mathrm{He}}$), ^{3}H ($^3\overline{\mathrm{H}}$), and $^3_\Lambda$H ($^3_{\overline{\Lambda}}\overline{\mathrm{H}}$) in ^{10}B+^{10}B, ^{12}C+^{12}C, ^{16}O+^{16}O, ^{20}Ne+^{20}Ne, ^{27}Al+^{27}Al, ^{40}Ar+^{40}Ar, ^{63}Cu+^{63}Cu, ^{96}Ru+^{96}Ru, ^{197}Au+^{197}Au, and ^{238}U+ ^{238}U collisions at $\sqrt{s_{\mathrm{NN}}}$ = 200 GeV calculated by PACIAE+DCPC model. One can see that our simulation results in different collision systems are compatible with the STAR [10,11,50,51] and PHENIX [52,53] experimental data within uncertainties for Au + Au collisions with a similar mean number of nucleon participants $\langle N_{\mathrm{part}} \rangle$. As is shown in Fig. 1a, b, the yield dN/dy of each particle species strongly depends on the size of the collision system, the yield dN/dy for each particle species appears to increase linearly with atomic mass number A. The features of yield dN/dy for (hyper-)nuclei and their corresponding anti-(hyper-)nuclei are found to be similar.

The yield ratios of d/p ($\bar{\mathrm{d}}/\bar{\mathrm{p}}$), ^{3}He/p ($^3\overline{\mathrm{He}}/\bar{\mathrm{p}}$), and ^{3}H/p ($^3\overline{\mathrm{H}}/\bar{\mathrm{p}}$) as functions of A are calculated by PACIAE+DCPC model in the above mentioned collision systems at $\sqrt{s_{\mathrm{NN}}}$ = 200 GeV, as shown in Fig. 2. The theoretical estimate values of d/p ($\sim 3.6 \times 10^{-3}$) and ^{3}He/p ($\sim 1.0 \times 10^{-5}$) from the thermal-statistical models [16] are indicated as dashed lines. For comparison, the measured ratios in Au + Au collisions form STAR [10,11] and PHENIX [52,53] and in Pb + Pb collisions from ALICE [14], are also presented. The yield values of d/p and ^{3}He/p from PACIAE+DCPC model are consistent with the available STAR, PHENIX, and ALICE data and the predicted values by the thermal-statistical models.

Figure 2 shows that the yield ratios of d/p ($\bar{\mathrm{d}}/\bar{\mathrm{p}}$), ^{3}He/p ($^3\overline{\mathrm{He}}/\bar{\mathrm{p}}$), and ^{3}H/p ($^3\overline{\mathrm{H}}/\bar{\mathrm{p}}$) first increases with the system size A rapidly and then almost saturates at large A. One can also obtain that ratios of ^{3}He/p ($^3\overline{\mathrm{He}}/\bar{\mathrm{p}}$), and ^{3}H/p ($^3\overline{\mathrm{H}}/\bar{\mathrm{p}}$) have

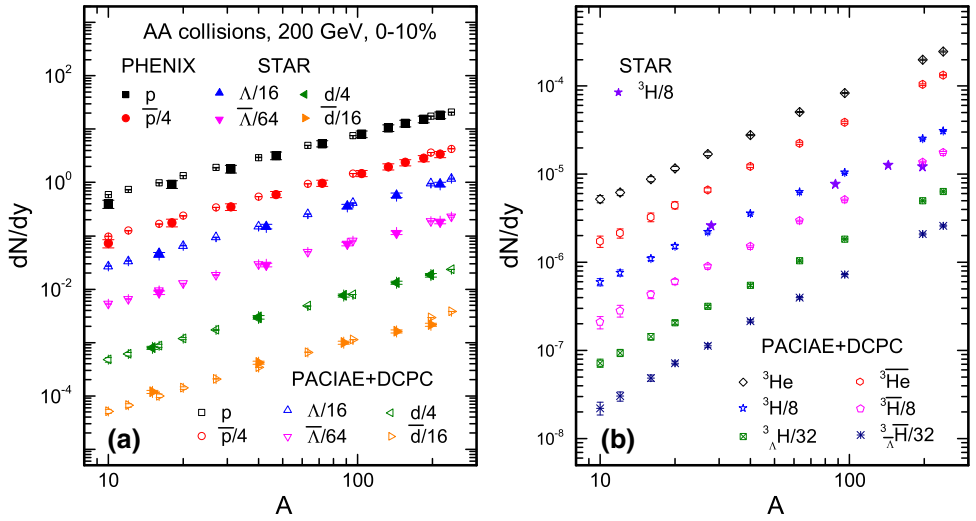

Fig. 1 The integrated yields dN/dy of particles in ^{10}B+^{10}B, ^{12}C+^{12}C, ^{16}O+^{16}O, ^{20}Ne+^{20}Ne, ^{27}Al+^{27}Al, ^{40}Ar+^{40}Ar, ^{63}Cu+^{63}Cu, ^{96}Ru+^{96}Ru, ^{197}Au+^{197}Au, and ^{238}U+^{238}U collisions at $\sqrt{s_{\rm NN}} = 200$ GeV calculated by PACIAE+DCPC model, **a** for p ($\bar{\rm p}$), Λ ($\bar{\Lambda}$), d ($\bar{\rm d}$), **b** for ^{3}He ($^3\overline{\rm He}$), ^{3}H ($^3\overline{\rm H}$), and $^3_\Lambda$H ($^3_{\bar{\Lambda}}\overline{\rm H}$), respectively. The STAR and PHENIX experimental data for Au + Au collisions are taken from [10,11,50–53]. For clarity the yield of Λ ($\bar{\Lambda}$), ^{3}He ($^3\overline{\rm He}$), and $^3_\Lambda$H ($^3_{\bar{\Lambda}}\overline{\rm H}$) are divided by an appropriate coefficient

a stronger system size dependence than the d/p ($\bar{\rm d}/\bar{\rm p}$) ratio, since ^{3}He ($^3\overline{\rm He}$) and ^{3}H ($^3\overline{\rm H}$) have three nucleons while d ($\bar{\rm d}$) has two nucleons. Another reason for this observation is that three-body (anti-)nuclei is more sensitive to the spatial distribution of nucleons in the emission source [54]. Besides, we can see from Fig. 2a, b that significant differences between d/p, ^{3}He/p, ^{3}H/p for nuclei and $\bar{\rm d}/\bar{\rm p}$, $^3\overline{\rm He}/\bar{\rm p}$, $^3\overline{\rm H}/\bar{\rm p}$ for anti-nuclei are present. This can be interpreted as production of light anti-nuclei is harder than that of light nuclei in high energy nuclear collisions at RHIC energy [14].

Similar to yield ratios of ^{3}He/p ($^3\overline{\rm He}/\bar{\rm p}$) and ^{3}H/p ($^3\overline{\rm H}/\bar{\rm p}$), the system size dependence of $^3_\Lambda$H/Λ ($^3_{\bar{\Lambda}}\overline{\rm H}/\bar{\Lambda}$) ratios in different collision systems at $\sqrt{s_{\rm NN}} = 200$ GeV are presented in panel (a) of Fig. 3. The dashed and solid curves represent fits using a simple function of $\log_{10}(Ratio) = p \cdot A^q$ for $^3_\Lambda$H/Λ and $^3_{\bar{\Lambda}}\overline{\rm H}/\bar{\Lambda}$ ratios, respectively. Experimental data from ALICE [15] are also shown by solid triangle with error bars. Comparing with Fig. 2b, we can find that the yield ratios $^3_\Lambda$H/Λ ($^3_{\bar{\Lambda}}\overline{H}/\bar{\Lambda}$) for (anti-)hypernuclei production are much more suppressed than the ^{3}He/p ($^3\overline{\rm He}/\bar{\rm p}$) and ^{3}H/p ($^3\overline{\rm H}/\bar{\rm p}$) ratios for light (anti-)nuclei production in high energy nuclear collisions at RHIC energy, though these two yield ratios have a similar trend increasing with A. The reasons of this suppression can be understood that (anti-)hypernuclei are more difficult to produce than light (anti-)nuclei for the same number of nucleons coalescence.

We then further investigate the strangeness population factor s_3, namely, a double ratio typically expressed as $s_3 = (^3_\Lambda{\rm H} \times {\rm p})/(^3{\rm He} \times \Lambda)$, which should be a value about one in a coalescence model [55]. It is a possible probe to study the properties of QGP matter created in high-energy nuclear

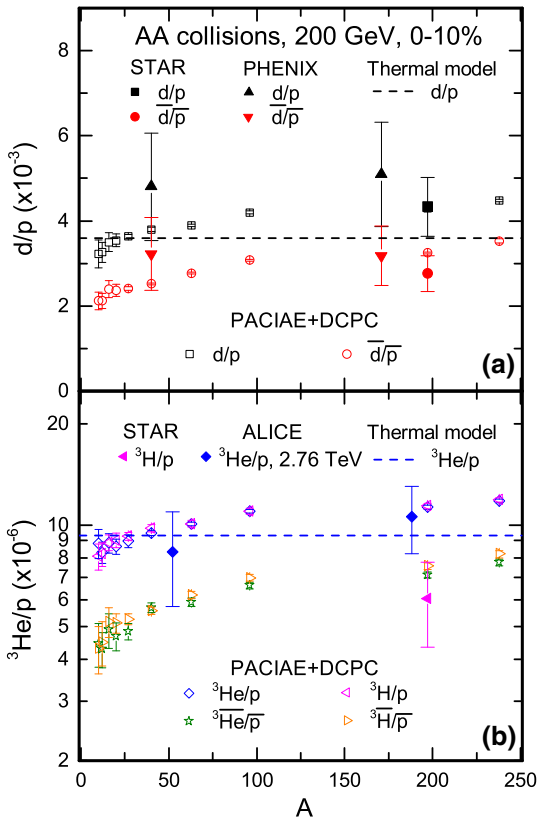

Fig. 2 The yield ratios of d/p ($\bar{\rm d}/\bar{\rm p}$), ^{3}He/p ($^3\overline{\rm He}/\bar{\rm p}$), and ^{3}H/p ($^3\overline{\rm H}/\bar{\rm p}$) in the scan of nuclear systems from ^{10}B+^{10}B to ^{238}U+^{238}U at $\sqrt{s_{\rm NN}} =$ 200 GeV calculated by PACIAE+DCPC model, represented by hollow points. The experimental data (solid points) were taken from STAR [10,11], PHENIX [52,53], and ALICE [14], respectively. The dashed lines are the estimate values of thermal-statistical models [16]. Here the vertical lines show statistical errors

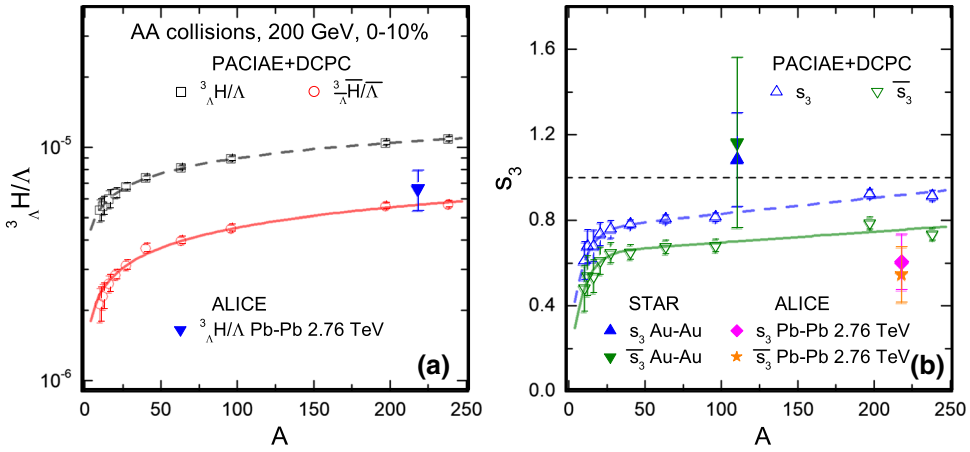

Fig. 3 The system size dependence of ${}^{3}_{\Lambda}\mathrm{H}/\Lambda$ (${}^{3}_{\Lambda}\overline{\mathrm{H}}/\overline{\Lambda}$) ratios **a** and strangeness population factor $s_3(\overline{s_3})$ **b** in different collision systems from ^{10}B+^{10}B to ^{238}U+^{238}U at $\sqrt{s_{\mathrm{NN}}} = 200$ GeV. The hollow points represent the results calculated using PACIAE+DCPC model, which the dashed and solid fitting curves represent for ratios of anti-(hyper-)nuclei and (hyper-)nuclei, respectively. Experimental data (solid points) from STAR and ALICE are taken from Refs. [12,15]. The error bars show statistical uncertainties

collisions, because of its sensitivity to the local baryon-strangeness correlation [56,57].

Figure 3b presents the system size dependence of strangeness population factor $s_3(\overline{s_3})$ by PACIAE+DCPC model in different collision systems at $\sqrt{s_{\mathrm{NN}}} = 200$ GeV. The STAR data for 0-80% Au + Au collisions and ALICE data for 0-10% Pb + Pb collisions taken from Refs. [12,15] are shown. As the fitted curves indicate, the values of $s_3(\overline{s_3})$ increase as A in 0-10% centrality nuclear collisions at RHIC energy. An obvious system size dependence of $s_3(\overline{s_3})$ is presented. In Ref. [54] a similar increase trend of s_3 with charged particle multiplicity $dN_{ch}/d\eta$ in Pb+Pb collisions is shown at LHC energy. Besides, the values of $s_3(\overline{s_3})$ by PACIAE+DCPC model are in agreement with available experimental data from STAR and ALICE within uncertainties.

However, one can also see that the increasing trend of $s_3(\overline{s_3})$ becomes saturated in the region of atomic mass number A about 12 to 27, i.e., there is a non-smooth A-dependence. In this region, the strangeness population factor $s_3(\overline{s_3})$ changes from a dramatically growing phase to a scenario that it only slightly varies with A. It has been argued for instance in Ref. [58] that, at the same energy, the density, the emitting source size, and the difference between the particle and anti-particle at freeze-out are important for the formation of (hyper-)nuclei in heavy ion collisions. Another research also showed that this three-body nuclei (hypertriton) is more sensitive to the spatial distribution of nucleons in the emission source [54]. By changing A of the colliding beam nuclei, the size of the emitting source can be varied in a wide range. It is therefore speculated that this non-smooth A-dependence can be largely determined by the variation of the relative size of the produced light nuclei compared to the emission source. Further studies are needed to fully understand this feature.

4 Conclusion

In the present paper, we have scanned the generation of light (anti-)nuclei and (anti-)hypertriton in 0-10% most central ^{10}B+^{10}B, ^{12}C+^{12}C, ^{16}O+^{16}O, ^{20}Ne+^{20}Ne, ^{27}Al+^{27}Al, ^{40}Ar+^{40}Ar, ^{63}Cu+^{63}Cu, ^{96}Ru+^{96}Ru, ^{197}Au+^{197}Au, and ^{238}U+^{238}U collisions at $\sqrt{s_{\mathrm{NN}}} = 200$ GeV using PACIAE+DCPC model. The yields, yield ratios, and strangeness population factors with atomic mass number A are predicted. The simulation results are well consistent with the available STAR, PHENIX, and ALICE experimental data within uncertainties.

The results show that the yield ratios of d/p ($\overline{\mathrm{d}}/\overline{\mathrm{p}}$), ^{3}He/p (${}^{3}\overline{\mathrm{He}}/\overline{\mathrm{p}}$) and ^{3}H/p (${}^{3}\overline{\mathrm{H}}/\overline{\mathrm{p}}$) for light (anti-)nuclei, as well as ${}^{3}_{\Lambda}\mathrm{H}/\Lambda$ (${}^{3}_{\Lambda}\overline{\mathrm{H}}/\overline{\Lambda}$) and double ratios $s_3(\overline{s_3})$ for (anti-)hypernuclei all have an obvious system size dependence, i.e., the ratio values increase with the increasing of atomic mass number A. There is a significant difference for yield ratios between (hyper)nuclei and their corresponding anti-(hyper)nuclei. Besides, the much stronger suppression of yield ratios for (anti-)hypernuclei than light (anti-)nuclei is presented in the collision system size scan programs at RHIC energy. A rapid growth of particle ratios and s_3 in the small collision systems ($A < 30$) is found in the system size scan. There exists a non-smooth A-dependence of s_3 in the region of A around 12 to 27. It can be related to the finite size effect of the emission source in different collision systems relative to the radius of the produced light nuclei.

Acknowledgements The work of G. Chen is supported by the National Natural Science Foundation of China (NSFC) (11475149), of L. Zheng is supported by the NSFC (11905188) and the Innovation Fund of Key Laboratory of Quark and Leption Physics QLPL2020P01, of D. M. Zhou is supported by the NSFC (11705167), and of Y. L. Xie is supported by the NSFC (12005196).

Data availability statement This manuscript has no associated data or the data will not be deposited. [Authors' comment: All data generated during this study are contained in this published article.]

References

1. J.H. Chen, D. Keane, Y.G. Ma et al., Phys. Rep. **760**, 1 (2018)
2. P. Braun-Munzinger, B. Dönigus, Nucl. Phys. A **987**, 144 (2019)
3. D. Oliinychenko, Nucl. Phys. A **1005**, 121754 (2021)
4. K.J. Sun, L.W. Chen, C.M. Ko et al., Phys. Lett. B **781**, 499 (2018)
5. K.J. Sun, F. Li, C.M. Ko, Phys. Lett. B **816**, 136258 (2021)
6. S. Acharya et al., (ALICE Collaboration), Phys. Lett. B **797**, 134905 (2019)
7. J. Adam et al., (STAR Collaboration), Nat. Phys. **16**, 409 (2020)
8. A. Kounine, S. Ting for the AMS Collaboration, PoS, **ICHEP2018**, 732(2019)
9. P. von Doetinchem, K. Perez, T. Aramaki et al., J. Cosmol. Astropart. Phys. **08**, 035 (2020)
10. J. Adam et al., (STAR Collaboration), Phys. Rev. C **99**, 064905 (2019)
11. D. Zhang for the STAR Collaboration, Nucl. Phys. A **1005**, 121825(2021)
12. B.I. Abelev et al., (STAR Collaboration), Science **328**, 58 (2010)
13. H. Agakishiev et al. (STAR Collaboration), Nat. (Lond.) **473**, 353 (2011)
14. J. Adam et al., (ALICE Collaboration), Phys. Rev. C **93**, 024917 (2016)
15. J. Adam et al., (ALICE Collaboration), Phys. Lett. B **754**, 360 (2016)
16. A. Andronic, P. Braun-Munzinger, J. Stachel et al., Phys. Lett. B **697**, 203 (2011)
17. V. Vovchenko, B. Dönigus, H. Stöecker, Phys. Lett. B **785**, 171 (2018)
18. A. Andronic, P. Braun-Munzinger, K. Redlich et al., Nature **561**, 321 (2018)
19. F. Bellini, A.P. Kalweit, Phys. Rev. C **99**, 054905 (2019)
20. N. Shah, Y.G. Ma, J.H. Chen et al., Phys. Lett. B **754**, 6 (2016)
21. M. Kachelrieß, S. Ostapchenko, J. Tjemsland, Eur. Phys. J. A **56**, 4 (2020)
22. W.B. Zhao, C. Shen, C.M. Ko et al., Phys. Rev. C **102**, 044912 (2020)
23. K.J. Sun, C.M. Ko, Z.W. Lin, Phys. Rev. C **103**, 064909 (2021)
24. Y. Oh, Z.W. Lin, C.M. Ko, Phys. Rev. C **80**, 064902 (2009)
25. D. Oliinychenko, L.G. Pang, H. Elfner et al., Phys. Rev. C **99**, 044907 (2019)
26. K.J. Sun, R. Wang, C.M. Ko et al., arXiv:2106.12742 (2021)
27. J. Staudenmaier, D. Oliinychenko, J.M. Torres-Rincon et al. Phys. Rev. C **104**, 034908 (2021)
28. S.L. Huang, Z.Y. Chen, W. Li et al., Phys. Rev. C **101**, 021901(R) (2020)
29. S. Zhang, Y.G. Ma, G.L. Ma et al., Phys. Lett. B **804**, 135366 (2020)
30. D.F. Wang, S. Zhang, Y.G. Ma, Phys. Rev. C **101**, 034906 (2020)
31. D.F. Wang, S. Zhang, Y.G. Ma, Phys. Rev. C **103**, 024901 (2021)
32. F. Becattini, J. Manninen, M. Gaździcki, Phys. Rev. C **73**, 044905 (2006)
33. M. Sievert, J. Noronha-Hostler, Phys. Rev. C **100**, 024904 (2019)
34. B. Schenke, C. Shen, P. Tribedy, Phys. Rev. C **102**, 044905 (2020)
35. Z.L. She, G. Chen, D.M. Zhou et al., Phys. Rev. C **103**, 014906 (2021)
36. B.H. Sa, D.M. Zhou, Y.L. Yan et al., Comput. Phys. Commun. **183**, 333 (2012); ibid, **224**, 412 (2018)
37. T. Sjöstrand, S. Mrenna, P. Skands, J. High Energy Phys. **05**, 026 (2006)
38. B.L. Combridge, J. Kripfgang, J. Ranft, Phys. Lett. B **70**, 234 (1977)
39. N.A. Ragab, Z.L. She, G. Chen, Eur. Phys. J. Plus **135**, 736 (2020)
40. H.G. Xu, G. Chen, Y.L. Yan et al., Phys. Rev. C **102**, 054319 (2020)
41. F.X. Liu, G. Chen, Z.L. She et al., Phys. Rev. C **99**, 034904 (2019)
42. F.X. Liu, G. Chen, Z.L. She et al., Eur. Phys. J. A **55**(9), 160 (2019)
43. G. Chen, Y.L. Yan, D.S. Li et al., Phys. Rev. C **86**, 054910 (2012)
44. G. Chen, H. Chen, J. Wu et al., Phys. Rev. C **88**, 034908 (2013)
45. G. Chen, H. Chen, J.L. Wang et al., J. Phys. G: Nucl. Part. Phys. **41**, 115102 (2014)
46. Z.J. Dong, Q.Y. Wang, G. Chen et al., Eur. Phys. J. A **54**, 144 (2018)
47. Z.L. She, G. Chen, H.G. Xu et al., Eur. Phys. J. A **52**, 93 (2016)
48. Z.L. She, G. Chen, D.M. Zhou et al., arXiv:1909.07070 (2019)
49. P. Liu, J.H. Chen, Y.G. Ma et al., Nucl. Sci. Tech. **28**, 55 (2017)
50. B.I. Abelev et al., (STAR Collaboration), Phys. Rev. C **79**, 034909 (2009)
51. G. Agakishiev et al., (STAR Collaboration), Phys. Rev. Lett. **108**, 072301 (2012)
52. S.S. Adler et al., (PHENIX Collaboration), Phys. Rev. C **69**, 034909 (2004)
53. S.S. Adler et al., (PHENIX Collaboration), Phys. Rev. Lett. **94**, 122302 (2005)
54. K.J. Sun, C.M. Ko, B. Dönigus, Phys. Lett. B **792**, 132 (2019)
55. T. Armstrong et al., (E864 Collaboration), Phys. Rev. C **70**, 024902 (2004)
56. S. Zhang, J.H. Chen, H. Crawford et al., Phys. Lett. B **684**, 224 (2010)
57. V. Koch, A. Majumder, J. Randrup, Phys. Rev. Lett. **95**, 182301 (2005)
58. A. Adare et al., (PHENIX Collaboration), arXiv:1410.2559 (2014)